Products and Mechanisms of the Reaction of Oleic Acid with Ozone and Nitrate Radical

Hui-Ming Hung, Yasmine Katrib, and Scot T. Martin*

Division of Engineering and Applied Sciences, 29 Oxford Street, Pierce Hall, Room 122, Harvard University, Cambridge, Massachusetts 02138

Received: January 6, 2005; In Final Form: March 11, 2005

The heterogeneous reactions of deposited, millimeter-sized oleic acid droplets with ozone and nitrate radicals are studied. Attenuated total reflectance infrared spectroscopy (ATR−IR), gas chromatography−mass spectrometry (GC−MS), and liquid chromatography−mass spectrometry (LC−MS) are used for product identification and quantification. The condensed-phase products of the ozonolysis of oleic acid droplets are 1-nonanal (30 ± 3% carbon yield), 9-oxononanoic acid (14 ± 2%), nonanoic acid (7 ± 1%), octanoic acid (1 ± 0.2%), azelaic acid (6 ± 3%), and unidentified products. The infrared spectra show that a major fraction of the unidentified products contain an ester group. Additionally, the mass spectra show that at least some of the unidentified products have molecular weights greater than 1000 amu, which implicates a polymerization reaction. The observed steps of 172 amu (9-oxononanoic acid) and 188 amu (azelaic acid Criegee intermediate) in the mass spectra suggest that these species are the monomers in the condensed-phase polymerization reactions. 9-Oxononanoic acid is proposed to lengthen the molecular chain via secondary ozonide formation; the azelaic acid Criegee intermediate links molecules units via ester formation (specifically, α-acyloxyalkyl hydroperoxides). For the reaction of oleic acid with nitrate radicals, functional groups including $-ONO_2$, $-O_2NO_2$, and $-NO_2$ are observed in the infrared spectra, and high molecular weight molecules are formed. Environmental scanning electron microscopy (ESEM) is employed to examine the hygroscopic properties of the oleic acid droplets before and after exposure to ozone or nitrate radical. After reaction, the droplets take up water at lower relative humidities compared to the unreacted droplets. The increased hygroscopic response may indicate that the oxidative aging of atmospheric organic aerosol particles has significant impact on radiative forcing.

1. Introduction

The chemical reactions of particle-phase organic molecules with gas-phase atmospheric oxidants leads to changes in the physicochemical properties of the atmospheric particles.[1,2] The oxidation of unsaturated organic matter, which increases the oxygen to carbon ratio,[3] often leads to greater hygroscopicity[4−6] and, consequently, can increase the tendency of atmospheric particles to take up water and nucleate clouds. These chemical reactions thereby influence radiative forcing and climate.[7] Moreover, in the oxidation reaction, volatile products may be released to the atmosphere, a process that may further affect gas-phase chemistry. Quantitative predictions of these impacts requires determining which products form and in what yields after exposure to oxidants and, furthermore, characterizing the hygroscopic properties of the reacted aerosol particles.

The reaction of oleic acid ($C_{18}H_{34}O_2$) with ozone has recently emerged as a model system to better understand the atmospheric chemical oxidation processes affecting organic particles. Reactive uptake coefficients,[8−14] product mechanisms,[13−17] particle hygroscopicity,[18] particle CCN activity,[19] and particle density[20] have been studied. The reaction proceeds via the addition of ozone to the double bond of oleic acid, which yields a primary ozonide (molozonide).[21] The high-energy ozonide rapidly decomposes. If the chemistry were completely analogous to gas-phase reactions, the associated products, each formed at 25% carbon-normalized yield, would be 1-nonanal, nonanoic acid, azelaic acid, and 9-oxononanoic acid.[9] Measurements, however, show 1-nonanal and 9-oxononaoic acid are major products whereas nonanoic acid and azelaic acid are minor products, as summarized in Table 1. Table 1 also shows that some studies find that 1-nonanal is largely a volatile product whereas other studies find significant amounts of 1-nonanal remain in the condensed phase. The question of why different experiments have observed different products and different yields needs to be answered to understand how to relate laboratory results to atmospheric particles.

An additional important recent discovery[13,15−17] is the formation of product compounds that have mass spectral peaks between 188 and 350 amu. The observed fragmentation pattern is not attributable to oleic acid (parent peak of 282 amu). Moreover, the instruments employed in these previous studies have an upper limit of approximately 350 amu so that higher mass peaks are not ruled out. Peaks at positions above 188 amu are significant because the highest molecular weight of four expected products is 188 amu from azelaic acid. The implication is that condensed-phase reaction pathways are more complex than simple ozonlysis and lead to high molecular weight compounds. The high molecular weight molecules are believed to arise from reactions involving oleic acid, reaction products, and Criegee intermediates; these pathways are significant only in condensed-phase reactions. Many questions remain, however, regarding the mechanism of these reactions and the characterization of the products. Another open question is how changes

* Corresponding author. E-mail: scot_martin@harvard.edu. Web: http://www.deas.harvard.edu/~smartin.

10.1021/jp0500900 CCC: $30.25
Published on Web 04/30/2005

TABLE 1: Summary of the Reaction Conditions and the Product Yields Reported in the Literature for the Ozonolysis of Oleic Acid[a]

				aerosol experiments		coated wall experiments					carbon-based yield of products (%)				
ref	oleic acid dimension (diameter or thickness)	ozone conc (molecules cm^{-3})	reacn time (s)	oleic acid conc (molecules cm^{-3})	oleic acid conc (molecules $particle^{-1}$)	flow ($cm^3\ s^{-1}$)	no. of molec of oleic acid	no. of molecules of ozone (intg'd quantity)	molar ratio of ozone to oleic acid	ozone exp'sre (atm s)	NN	OA	AA	NA	other
8	200−600 nm	2.5×10^{14}	7	$<2 \times 10^{12}$ [b]	$(8-200) \times 10^6$				$>10^2$	7×10^{-5}	n/a	n/a	n/a	n/a	
9, 43	10^3 μm	1.0×10^{14}	0.1			50−200	1.9×10^{21}	1.0×10^{15}	10^{-6}	4×10^{-7}	25[c]	n/a	p	p	
10	1.4−4.9 μm	3.4×10^{15}	8	$<1 \times 10^{14}$ [d]	$(3-100) \times 10^9$				>30	1×10^{-3}	n/a	p	n/a	n/a	
12	ca. 50 μm	$10^{11}-10^{12}$	>0.1			1.8	2×10^{21}	$>2 \times 10^{10}$	$>10^{-11}$	$>10^{-9}$	25[c]	n/a	n/a	n/a	
15, 20	2−30 nm	2.5×10^{14}	3	3×10^8 [e]	3×10^6 [e]				10^6	1×10^{-5}	0[f]	35[e]	2[e]	2[e]	35% yield of $C_xH_yO_z$ products; increase in density by 25%
18	ca. 100 μm	$10^{14}-10^{16}$	300			17	2.1×10^{17}	3×10^{19} [g]	140[g]	8×10^{-2} [g]	n/a	n/a	n/a	n/a	increase in water uptake at 95% relative humidity[f]
13	0.6−1.0 μm	2.5×10^{15}	4	$<5 \times 10^{13}$ [h]	5×10^8				>50	4×10^{-4}	42[i,j]	42[i]	6	9[i]	1% yield of 9-oxooctadecanoic acid
19	161 nm	1.0×10^{16}	300	$<4 \times 10^{10}$ [b]	4×10^6				$>2 \times 10^5$	4×10^{-1}	n/a	n/a	n/a	n/a	increase in CCN activity but only for high ozone exposure
16	155 nm	4.5×10^{15}	10	4×10^{11}	4×10^6				1×10^4	2×10^{-3}	P	p	p	p	cyclic oxygenates having oxygen−oxygen moieties, including secondary ozonides and cyclic geminal diperoxides
14	0.6−1.2 μm	2.5×10^{14} to 2.5×10^{15}	4	$<5 \times 10^{13}$ [h,k]	5×10^8				>50[k]	4×10^{-4} [j]	n/a	n/a	n/a	n/a	uptake results suggest 36% of oleic acid loss because of reactions with Criegee intermediates
17	polydisperse, submicron	7.0×10^{13}	300	4×10^{12}	n/a				18	8×10^{-4}	0[f]	p	p	0	major products include α−acyloxyalkyl hydroperoxides, secondary ozonides, α-alkoxyalkyl hydroperoxides, and oxocarboxylic acids
this work	0.5−3 mm	7.5×10^{15}	2000			1.7	1.9×10^{18}	3×10^{19}	16	1	30[f]	14	6	7	major yield of ester polymerization products of high molecular weight (specifically, α-acyloxyalkyl hydroperoxides); 1% yield of octanoic acid

[a] The designation "n/a" indicates that the analysis method was not performed for these chemical species. "p" indicates the chemical species was present but its yield was not quantified. (Conversion factors: 1 ppm = 10^{-6} atm = 2.5×10^{13} molecules cm^{-3} at 1 atm total pressure and 298 K. Key: OL, oleic acid; OA, 9-oxononanoic acid; AA, azelaic acid; NA, nonanoic acid; and NN, 1-nonanal.) [b] Assumption is made of an upper limit of 10^4 particles cm^{-3} based upon use of electrostatic classification of a polydisperse source. [c] Gas-phase 1-nonanal. [d] Assumption is made of an upper limit of 10^3 particles cm^{-3} based upon use of vibrating orifice aerosol generator. [e] Results are shown for 30 nm coating. [f] Condensed-phase 1-nonanal. [g] A range of ozone concentrations was used. Results are summarized for 6.5×10^{14} molecules of O_3 cm^{-3}. [h] Assumption is made of an upper limit of 10^5 particles cm^{-3} based upon use of a Meinhard TR-30-A1 polydisperse source. [i] These yields are tentative because relative detection sensitivities are assumed. See original publication. [j] Combined condensed-phase and gas-phase 1-nonanal. [k] 800-nm particles and 2.5×10^{15} molecules of O_3 cm^{-3} are employed for these calculations.

in physical properties, such as hygroscopicity and viscosity, depend on the nature of the oxidant, such as nitrate radical versus ozone, and on the specific products formed.

This paper addresses the foregoing questions. Results from attenuated total reflectance infrared spectroscopy (ATR−IR), gas-chromatography mass spectrometry (GC−MS), liquid-chromatography mass spectrometry (LC−MS), and environmental scanning electron microscopy (ESEM) are combined to examine the reactions of supported millimeter-sized oleic acid droplets with nitrate radical and ozone. The methodologies of identifying functional groups by infrared spectroscopy and of specific molecules by chromatography are highly complementary and have been applied before in the study of secondary organic aerosol.[22−24]

2. Experimental Approach

2.1. Preparation of Oleic Acid Droplets. Oleic acid droplets (>99% purity, Aldrich) are prepared with a micropipettor and dispensed onto a single-crystal germanium surface (Pike Technologies; Trapezoid shape of 56 mm long, 10 mm wide, and 4 mm thick). The droplet diameter is controllable from 0.5 to 3 mm. In a fine droplet experiment, for example, 1.5 μL of oleic acid is divided into hundreds of droplets, which have an average diameter of 0.5 mm. In a large droplet experiment, 1.5 μL of oleic acid is divided into 12 droplets. The average horizontal diameter of these droplets is approximately 2.7 mm, and a typical height of the droplets on the germanium support is 20 μm. The droplet diameter is measured via digital images taken with a camera.

2.2. Generation of Gas-Phase Oxidants. Ozone and nitrate radical are the gas-phase oxidants employed in this study. Ozone is generated via a commercial ozone generator (section 2.2.1). Nitrate radical is synthesized in the laboratory via the reaction of nitrogen dioxide with ozone (section 2.2.2).

2.2.1. Ozone. Ozone is generated by flowing dry air at 100 mL/min and 298 K through a UV light source (254 nm; Jelight source, Model 600). The ozone partial pressure in the effluent is measured via light absorbance and application of Beer's law. For this purpose, a Hg line lamp (254 nm) and a photodiode detector are employed along a 1-cm path length. An absorbance cross-section of 1.15×10^{-17} cm^2 molecule^{-1} is used in the calculations.[1] Ozonolysis of oleic acid is studied by exposure of supported droplets (section 2.1) to 30 or 300 ppm of ozone in air at 298 K.

2.2.2. Nitrate Radical. The thermal decomposition of N_2O_5 at 298 K is the source of nitrate radical in our experiments.[25−29] A reservoir of N_2O_5 is synthesized through the reaction of NO_2 with O_3 and stored cold:

$$NO_2 + O_3 \rightarrow NO_3 + O_2 \quad (1)$$

$$NO_2 + NO_3 \rightleftarrows N_2O_5 \quad (2)$$

The synthesis is carried out in a 1-L heavy-wall borosilicate glass bottle (ACE Glass, part #5414−15). There are three PTFE valves with Tefzel keys to control the addition of NO_2, the addition of O_3, and the release to vacuum. NO_2 (99.5% purity, Matheson Gas Product) is first introduced into the evacuated bottle until a brown color is visible. The bottle is then placed into a dry ice/acetone bath (195 K) to freeze the NO_2 gas. Once the NO_2 is frozen, the release is opened to vacuum, which removes any residual gas-phase species in the bottle. The bottle is then removed from the cooling bath, warmed, and filled with approximately 7 psi of O_3, which is generated by flowing 50 mL of O_2/min through an electrode discharge (Anderson group, Harvard University). The chemistry shown in eqs 1 and 2 ensues, although initially not to completion. After 15 min, the bottle is returned to the dry ice/acetone bath to trap the produced N_2O_5 and the residual NO_2 as solids. The cycle of the removal of gas-phase species by vacuum release, ozone addition, chemical reaction, and freezing is repeated until the NO_2 is completely reacted. The endpoint is determined by visual observation at room temperature because gaseous NO_2 is brown whereas N_2O_5 is colorless. When the synthesis is complete, the N_2O_5 is stored at 195 K until needed for experiments (up to 7 days).

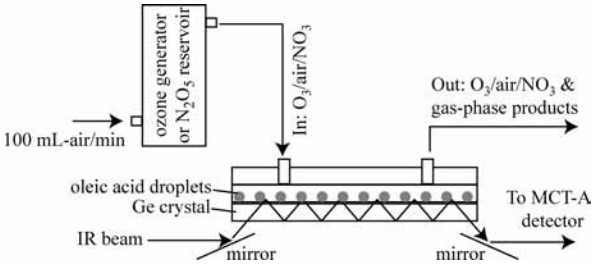

Figure 1. Schematic diagram of the attenuated total reflectance infrared spectroscopy (ATR−IR) apparatus.

The reaction of oleic acid with nitrate radical is studied by exposure of supported droplets (section 2.1) to nitrate radical in air at 298 K. In a typical experiment, the NO_3 radical is introduced by flowing 100 mL/min of dry air through the N_2O_5 reservoir. The N_2O_5 vapor decomposes to form NO_3 radical and NO_2 (eq 2). The equilibration is rapid at 298 K (rate constant of 0.05 s^{-1}).[30] The equilibrium relationship is 5.5×10^{-27} exp(10724/T) = [N_2O_5]/([NO_2][NO_3]) (cm^3 molecule^{-1}).[31] Depending upon the desired NO_3 concentration, the reservoir bottle is held at a bath filled with either dry ice/acetone, which ensures good thermal contact and a reservoir temperature of 195 K, or dry ice only, which has poor thermal contact and leads to a reservoir temperature above 195 K and thus a higher N_2O_5 vapor pressure and, via eq2, a higher NO_3 concentration. For example, saturated N_2O_5 vapor pressure varies from 0.006 Torr at 208 K to 0.254 Torr at 223 K. Correspondingly, 0.1 ppm (7.6×10^{-5} Torr) and 0.8 ppm of NO_3 radical result at 298 K; these concentrations are calculated by employing the equilibrium equation provided above for the relationships among [NO_2], [NO_3], and [N_2O_5]. In our experiments, we do not directly measure the NO_3 concentration, so we call our experiments "low NO_3" (case of good thermal contact) and "high NO_3" (case of poor thermal contact). In addition, HNO_3 impurity is commonly present in this preparation method.

2.3. Analytical Methods.

2.3.1. Infrared Spectroscopy. The oxidation reactions of oleic acid droplets with ozone and nitrate radical are monitored in real time by employing attenuated total reflectance infrared spectroscopy (ATR−IR) (Figure 1). The oleic acid droplets reside on a germanium crystal, through which the infrared light propagates. At every reflection, the evanescent wave probes the droplets. The penetration depth of the evanescent wave is approximately one micron. The collected spectra are, therefore, sensitive only to the condensed-phase reaction products and not to any volatilized reaction products. The infrared absorbance spectra are collected using a Nicolet Nexus 670 FT-IR set to a resolution of 2 cm^{-1}, a spectral range of 500−6000 cm^{-1}, and an averaging of 16 scans. A clean germanium crystal is used for the background spectrum.

The infrared spectra provide information on the presence and the absence of chemical functional groups. Reference infrared

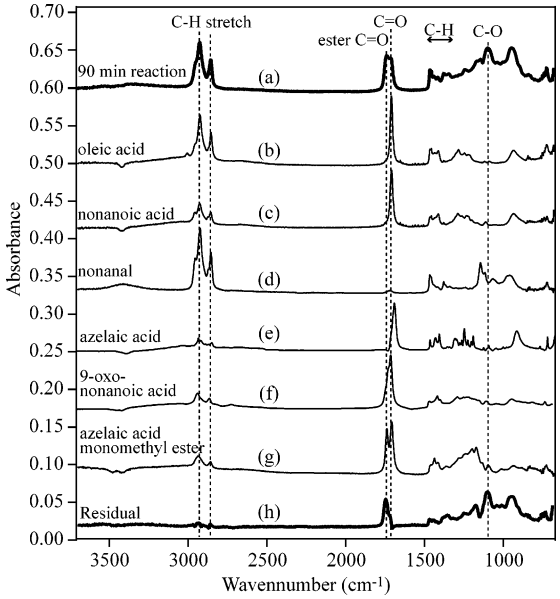

Figure 2. Infrared spectra of (a) oleic acid droplets after reaction with ozone (90 min, 300 ppm O_3, 2.7-mm droplets) to the spectra of pure compounds of (b) oleic acid, (c) nonanoic acid, (d) 1-nonanal, (e) azelaic acid, (f) 9-oxononanoic acid, (g) an ester (azelaic acid monomethyl ester), and (h) residual after linear analysis (see text). The spectra are offset for clarity.

spectra (shown in Figure 2) are collected for oleic acid (>99% purity, Aldrich), nonanoic acid (98% purity, Aldrich), 1-nonanal (98% purity, Aldrich), azelaic acid (98% purity, Aldrich), 9-oxononanoic acid (>99% purity, Larodan, Sweden), and azelaic acid monomethyl ester (85% purity, Aldrich). Azelaic acid is a solid at room temperatures. The other chemicals are liquids. For the liquids, a 1.5 μL sample is dispersed as 12 droplets on to the geranium crystal (section 2.1). Azelaic acid is dissolved in acetone until saturation of the solution; these liquid droplets are dispersed on the germanium crystal, and the infrared spectrum is recorded after the acetone evaporates.

2.3.2. Chromatography. The reacted droplets are collected from the germanium crystal for analysis by GC−MS and LC−MS to obtain further product information. The droplets are dissolved in acetone for GC−MS analysis and in acetonitrile for the LC−MS analysis.

The GC−MS is an HP 6890 series GC equipped with an HP 5973 mass selective detector (injection volume of 0.2 μL controlled by an autosampler, HP1 column #19091Z-433, helium carrier gas). The oven temperature program is 50 °C for 2 min, 20 °C/min until 325 °C, and 325 °C for 2 min. The electron impact mass spectrum of each peak is searched in the NIST mass spectrum database. In addition, authentic standards for concentration calibration are also prepared to quantify the product yields of 1-nonanal, nonanoic acid, octanoic acid, and oleic acid. The ionization efficiency of 9-oxononanoic acid is taken as the average of the other calibration species, which is supported by the calibration measurements of Katrib et al.[15] A pure standard of azelaic acid shows that the analysis method is not sensitive to this compound.

A Micromass LCT equipped with a Genesis reversed-phase C18 column is employed for LC−MS analysis. Nebulization and ionization are by electrospray, and mass analysis is by time of flight. The carrier solvent (0.35 mL/min) is a mixture of water and acetonitrile. The gradient program begins as 5% acetonitrile for 1 min, which is increased linearly to 100% acetonitrile by 9 min, held there until 13 min, decreased linearly to 10% acetonitrile by 14 min, and further decreased to 5% acetonitrile by 16 min. Using pure standards, we find that this method is sensitive to azelaic acid, 9-oxononanoic acid, and other high mass species but not to 1-nonanal, nonanoic acid, and oleic acid.

2.4. Environmental Scanning Electron Microscopy. The hygroscopic properties of unreacted and reacted oleic acid droplets are studied using an FEI Quanta 200 environmental scanning electron microscope (ESEM). Water vapor is employed as the image gas. The sample is prepared either by transferring reacted droplets from the germanium crystal to a glass slip (method 1) or by dispersing 0.1 μL of oleic acid onto a glass slip followed by exposure to oxidants (method 2).

The hygroscopic properties of the reacted droplets are observed by varying the water partial pressure in the ESEM chamber.[32] After each adjustment of the water partial pressure, an image is recorded after 2 min of equilibration. To reduce possible damage of the sample by the electron beam, the images are taken at low magnification (less than $\times$1000), and the electron beam is blocked during equilibration.

The temperature of the sample is controlled by a peltier stage set at 2 °C. Due to a possible temperature gradient between the peltier stage and the glass slip, the temperature on the glass slip is calibrated by the NaCl deliquescence point (75% RH). Observed deliquescence at 4.35 Torr implies that the NaCl particles on the glass slip have a temperature of 3.3 °C. The reacted and unreacted oleic acid droplets are also assumed to be at 3.3 ± 0.5 °C.

3. Results and Discussion

Changes in the hygroscopic properties of oleic acid after reaction with ozone and nitrate radical and the corresponding changes in viscosity are presented in sections 3.1 and 3.2, respectively. The products and the mechanism of the reaction with nitrate radical and ozone are subsequently presented in sections 3.3. and 3.4.

3.1. Hygroscopic Properties of Unreacted versus Reacted Oleic Acid Droplets. The hygroscopic properties of oleic acid droplets before and after reaction with ozone or nitrate radical are investigated at 3.3 °C in the ESEM. Unreacted particles do not take up observable water even at 99% RH (Figure 3a). Droplets reacted with ozone (0.16 atm s) at first do not show any significant water uptake (results not shown); however, after 3 days storage in a desiccator without further exposure to ozone, the reacted droplets take up water at 91 ± 1% RH (Figure 3b). The apparent implication is that a combination of evaporation of nonpolar products and continued condensed-phase reactions after the initial ozonlysis result in increased particle hygroscopicity after several days. In comparison, droplets reacted with NO_3 radical take up water at 97 ± 1% RH when first observed in the ESEM (Figure 3c).

Hygroscopicity was also observed to increase by Asad et al.[18] and Broekhuizen et al.[19] following exposure of oleic acid to ozone. Asad et al.[18] detected significant water uptake at 95% RH for an oleic acid film exposed to 270 ppm O_3 in 1 bar O_2 for 5 min (0.081 atm s). Broekhuizen et al.[19] reported that unreacted (0 atm s) and ozone-reacted (0.013 atm s) oleic acid particles are CCN inactive up to supersaturations of 0.6% but become highly CCN active after exposure to 0.42 atm s of ozone. The ratio of moles of ozone to moles of oleic acid was 10^1 for the current study, 10^2 for Asad et al.,[18] and 10^5 for Broekhuizen et al.[19] (cf. Table 1).

3.2. Qualitative Observations of Increased Viscosity. Visual observations of the flow characteristics and the stickiness of the droplets show qualitatively that droplet viscosity increases after the reaction with ozone or nitrate radical. An increased

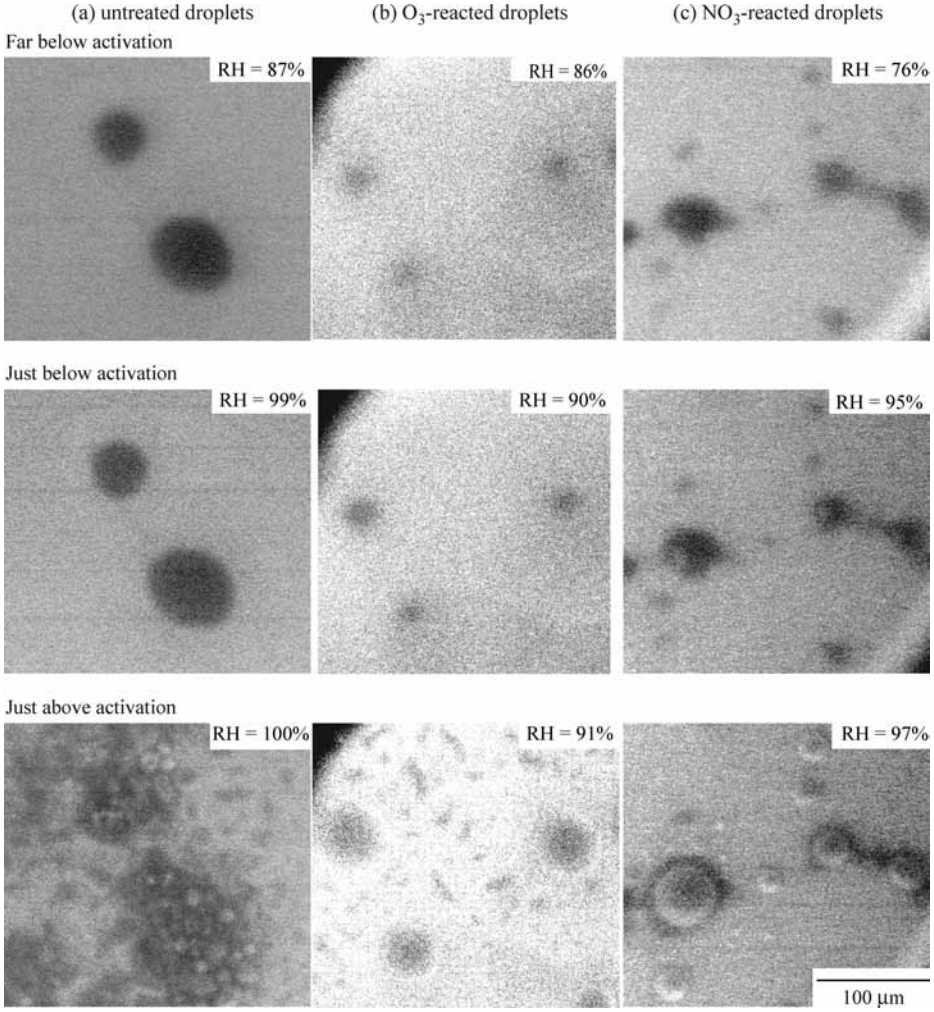

Figure 3. Micrographs obtained by environmental scanning electron microscopy (ESEM). Columns show images collected of (a) untreated oleic acid droplets, (b) O_3-treated droplets (method 1; see section 2.4), and (c) NO_3-treated droplets (method 2). Rows, shown for increasing relative humidity, reveal that hygroscopic droplet growth occurs at an activation relative humidity. The precise humidity depends on droplet treatment (i.e., O_3 or NO_3 exposure). Conditions: (b) exposure to 90 min of 300 ppm O_3 followed by 3 days storage and (c) exposure to NO_3 as "low NO_3" (224 min) → "high NO_3" (55 min) → "low NO_3" (52 min) → 0 ppm (70 min) followed by two months storage. The images are adjusted in *Adobe Photoshop* to improve contrast and brightness.

viscosity is consistent with two processes believed active in oleic acid ozonolysis, which are the formation of high molecular weight products[13−17] and an increase in intermolecular bonding associated with the formation of carboxylic acid, ketone, aldehydes, and other oxygen-bearing chemical functionalities.[3] Moreover, the droplets reacted with ozone become a dry solid when stored in the desiccator for one week, which is consistent with both further evaporation of the reaction products and continued condensed-phase reactions, as also inferred from the ESEM observations. In contrast, the droplets reacted with nitrate radical remain liquid, at least for the two months of our observation period.

3.3. Products and Mechanism of the Reaction of Oleic Acid with Nitrate Radical. The nitrate radical can add across the double bond of oleic acid to form organic nitrates.[27,33−36] Direct evidence of these species is provided by the infrared spectra shown in Figure 4. Peaks A1 (1645 cm^{-1}), A2 (1278 cm^{-1}), and A3 (843 cm^{-1}) are attributable to organonitrate ($-ONO_2$) functional groups.[37] Peaks B (1553 cm^{-1}) and C (1364 cm^{-1}) are consistent with organonitro ($-NO_2$) functional groups.[38] Organoperoxynitrates ($-O_2NO_2$) also absorb at 1296 cm^{-1}.[31] The apparent absence of the 790 cm^{-1} peak, which is also characteristic of organoperoxynitrates, though at lower intensity, might be due to a blue-shift into the shoulder of peak A3 for the ATR measurements[39] of this study compared to gas-phase transmission measurements of Wangberg (1997).[31] Peaks A−D have similar temporal profiles (Figure 5), which is suggestive of common pathways of chemical formation. Moreover, these peaks are absent before reaction and increase greatly after reaction. The temporal profiles further show that peaks A−D increase linearly with total exposure to nitrate radical, at least until 280 min when no further changes are observed, possibly because the reactive double bonds of oleic acid are depleted.

Peak E at 1710 cm^{-1} is attributable to the C═O vibration of ketones, aldehydes, and carboxylic acids as well as organoperoxynitrates. As a point of fact, so long as carboxylic acids are present, their behavior dominates changes in the C═O absorption (1710 cm^{-1}) because of their 100-fold greater oscillation strength compared to aldehydes and ketones.[23,24] The similar temporal behavior of peak E with peaks A−D (Figure 5) suggests that a combination of ketones, aldehydes, carboxylic acids, and nitro-, nitrate-, and peroxynitrate-organics form contemporaneously in the reaction of oleic acid with nitrate radical.

In contrast to the monotonic temporal behavior of peaks A−E, the intensities of peaks F (1805 cm^{-1}), G (1029 cm^{-1}), and H (789 cm^{-1}) at first increase and then subsequently decrease

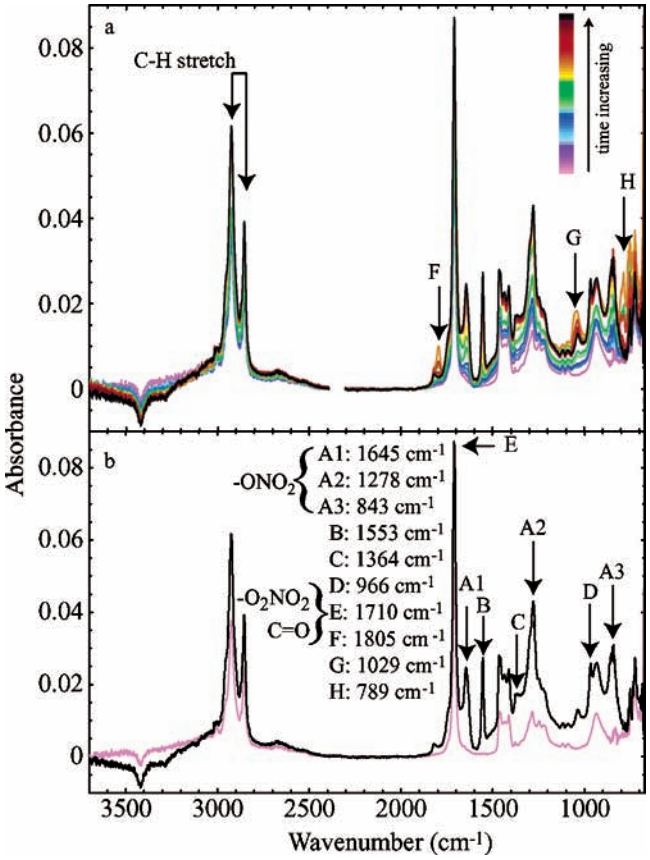

Figure 4. (a) Infrared spectra recorded during the reaction of oleic acid droplets with nitrate radical. The time profile of NO_3 is described in Figure 3. Conditions: 100 mL of air/min flow, 1 atm, and 298 K. (b) Spectra from *a* shown for 0 and 500 min of NO_3 exposure.

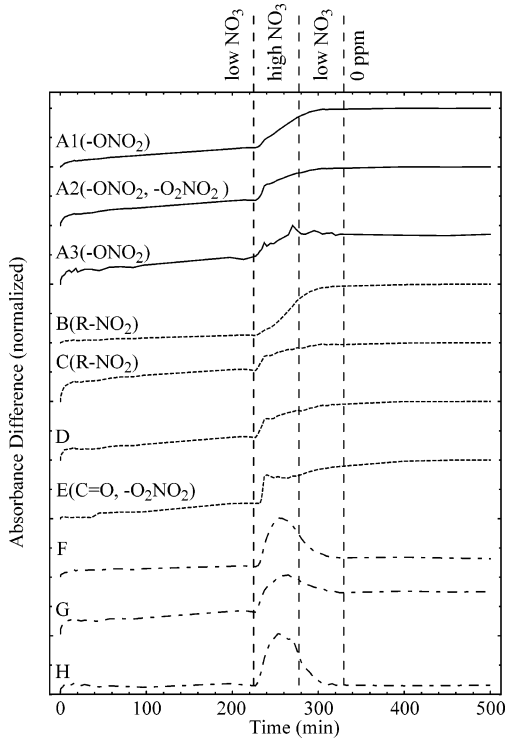

Figure 5. Temporal response for several regions of the infrared spectra shown in Figure 4.

during the exposure of oleic acid to NO_3. The implication is that reactive intermediates first form from nitrate radical addition and that these intermediates rapidly react to form further products. Any proposed chemical mechanism should account for this behavior.

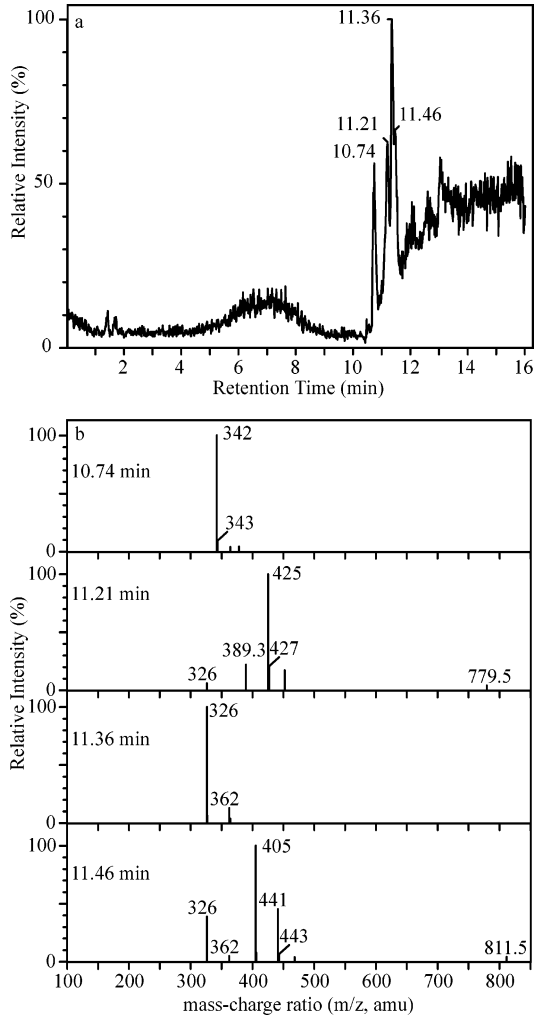

Figure 6. (a) HPLC−MS chromatogram of acetonitrile-soluble constituents of oleic acid droplets after reaction with nitrate radical (500 min). The MS is operated in negative ion mode. The time profile of P_{NO_3} is the same as described for Figure 3. (b) Electrospray mass spectra for the peaks shown in the chromatogram.

The general information about functional groups, which is based upon the infrared data, is complemented by specific, if incomplete, product identification by LC−MS analyses. The LC−MS chromatogram of acetonitrile-soluble constituents and the mass spectra corresponding to peaks in the chromatogram are shown in Figure 6 after 330 min of exposure to nitrate radical and storage for 7 days. The absence of detectable quantities of the usual ozonolysis products (e.g., 9-oxononanoic acid) indicates that the reaction pathways of nitrate radical and oleic acid differ markedly from those of ozonolysis. In fact, none of the major ozonolysis products is detected in significant quantities by GC−MS (data not shown) or LC−MS analyses.

The four major peaks in the LC−MS chromatogram and their corresponding mass spectra show that the nitrate radical reactions form long chain carbon molecules. The mass spectra have peaks from 326 amu up to 811 amu. Although the peak at 779 amu possibly arises from a dimer of 389 amu with a proton and the peak at 811 amu could be accounted for by a dimer of 405 plus a proton,[40] the peaks above 422 amu such as 427 or 443 amu are sufficient to conclude that long chain molecules form. The parent compound of oleic acid has a molecular weight of 282 amu, and nitrated scission products have molecular weights of up to 247 amu (cf. Figure 7). A possible nonscission

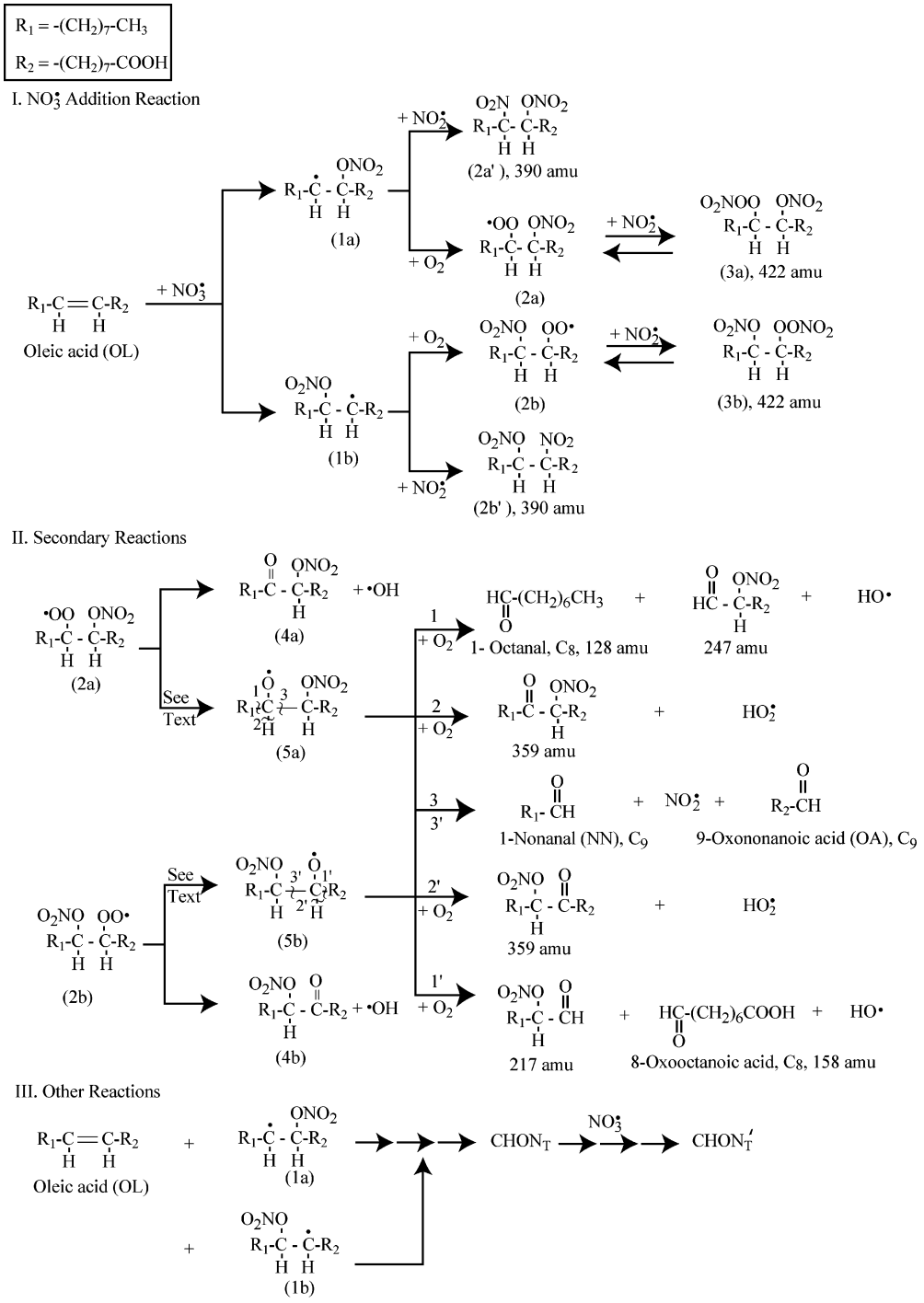

Figure 7. Proposed chemical mechanism for the reactions of nitrate radical with ozone. ($CHNO_T$ denotes products formed by addition pathways of radical intermediates across the double bond of oleic acid. The compounds are analogous to CHO_T proposed by Katrib et al.[15])

peroxynitrate species has a molecular weight of up to 422 amu. Many peaks are, however, observed at higher amu values (Figure 6). Therefore, we conclude that long chain carbon molecules are formed in the reaction of nitrate radical with oleic acid.

The mechanism we propose for the nitrate radical reaction is shown in Figure 7. In the first step, two nitrooxy substituted alkyl radicals form from nitrate radical addition across the double bond of oleic acid (labeled 1a and 1b in Figure 7). (The alternative pathway of hydrogen abstraction by NO_3 radical is slower.[36]) In the presence of molecular oxygen, the alkyl radicals form alkylperoxy radicals (labeled 2a and 2b).[27] Peroxynitrates can form (labeled 3a and 3b) if the alkylperoxy radicals combine with NO_2. The alkyl radicals can also react with NO_2 to form nitro products 2a′ and 2b′. Alternatively, the alkylperoxy radicals can form aldehyde species (4a and 4b) or may react with NO_2, NO_3, HO_2, or other peroxy radicals to give oxo-radicals[41] (5a and 5b). Species 5a and 5b can decompose by three different pathways, and eight different stable products could form (cf. Figure 7). The formation of some of these products may account for the changes observed in the infrared spectra. Pathways 3′ and 3 would lead to 1-nonanal and 9-oxononanoic acid, which are major products of ozonolysis. The final aspect of the proposed mechanism is the formation of long chain products, which may result from the addition of the primary products 1a and 1b to the double bonds of another oleic acid molecule (cf. part III of Figure 7).

In comparison to ozonolysis, a key difference for the reactions of nitrate radical with oleic acid is the absence of a high energy

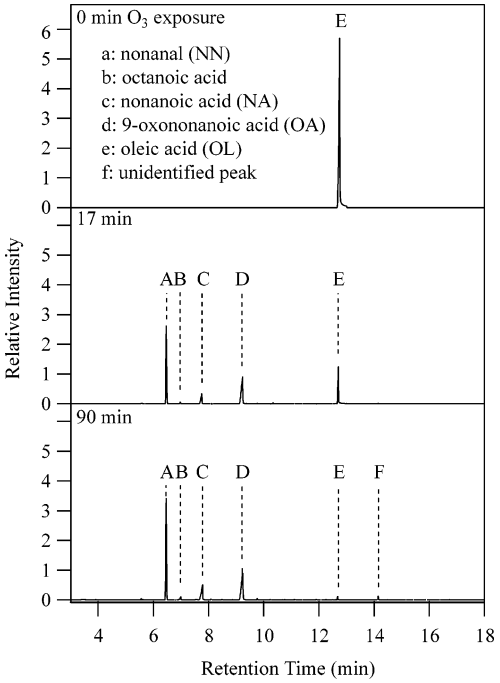

Figure 8. GC−MS chromatograms of acetone-soluble constituents of oleic acid droplets after reaction with ozone for three exposure times. Oleic acid, 1-nonanal, nonanoic acid, octanoic acid, and 9-oxononanoic acid are identified. Control runs show that this method is not sensitive to azeleic acid. Conditions: 300 ppm O_3, 100 mL of air/min flow, 1 atm, 298 K, and 2.7-mm droplets.

molonozide that cleaves to form two C_9 products from a C_{18} parent. Instead, in the case of nitrate radical, a stable C_{18} product may form by addition of NO_2 to the initial intermediate, or, if the C−C bond cleaves, C_8 and C_{10} products are expected via pathways 1 and 1′, a C_{18} product via pathways 2 and 2′, and two C_9 products via pathways 3 and 3′.

3.4. Products and Mechanism of the Ozonolysis of Oleic Acid.

3.4.1. Product Identification. GC−MS chromatograms of the acetone-soluble constituents of the reacted droplets are shown in Figure 8 for three different ozone exposure times (0, 17, and 90 min with 300 ppm O_3). As expected, oleic acid decreases with increasing ozone exposure time. Concurrently, the concentrations of condensed-phase ozonolysis products increase. For 90 min of ozone exposure, these products include 1-nonanal (30 ± 3% carbon yield), 9-oxononanoic acid (14 ± 2% carbon yield), nonanoic acid (7 ± 1% carbon yield), and octanoic acid (approximately 1% carbon yield). The remaining 48 ± 5% of carbon possibly occurs as gas-phase products, as condensed-phase species not detected by the GC−MS analysis, or as species not soluble in acetone. The time evolution of parent loss and product yield is shown in Figure 9. The decrease in oleic acid follows an exponential decay, with an empirical first-order rate coefficient of 0.12 min^{-1}.

The LC−MS results show the formation of azelaic acid (6 ± 3%), 9-oxononanoic acid (not quantified), and other unidentified species that have peaks of up to 1039 amu (Figure 10). The mass spectra at 11.0, 11.5, and 12.6 min have peaks spaced at 172 (173) and 188 (189) amu, which are the molecular weights of 9-oxononanoic acid (plus H^+) and azelaic acid (plus H^+), respectively. Moreover, the product at 9.0 min has a peak at 550 amu, which could be composed of the product at 8.6 min (378 amu) joined to 9-oxononanoic acid (172 amu). The product at 11.0 min has a peak at 708 amu, which may have been formed by the product at 10.8 min (520 amu) plus azelaic acid (188 amu). The LC−MS data therefore strongly suggest that polymerization occurs during the ozonolysis of oleic acid droplets.

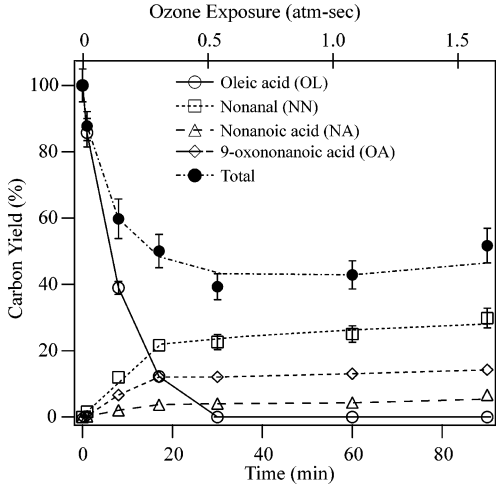

Figure 9. Percent loss of oleic acid and percent yield of products with increasing ozone exposure (GC−MS analysis; not sensitive to azeleic acid). Conditions: same as in Figure 8. "Total" is the sum of concentrations of OL, NN, NA, and OA.

The infrared spectra recorded during the ozonolysis of oleic acid droplets are shown in Figure 11. As ozone exposure increases, the IR spectra show the disappearance of oleic acid and the formation of condensed-phase products. The infrared spectra of reference condensed-phase species are shown in Figure 2. The infrared spectra of the pure compounds are assumed to be representative of the IR spectra of those same compounds when mixed together in the reacted particles. Azelaic acid monomethyl ester is chosen as a reference species to illustrate the C═O vibration peak at 1740 cm^{-1} and the C−O vibration peak at 1100 cm^{-1} of an ester.[42] A similar peak also appears in the spectrum of the oleic acid droplets after ozonolysis. The absorbance from 1330 to 1470 cm^{-1} arises from methyl and methlyene groups.[42]

The product spectrum in Figure 2a, which is similar to that recorded by Asad et al.,[18] is analyzed by us via a linear statistical model for possible contributions by oleic acid (OL), nonanal (NN), 9-oxononanoic acid (OA), azelaic acid (AA), and nonanoic acid (NA). NN and OA contribute substantially to the product spectrum, and the residual spectrum obtained from a basis set of just NN and OA is shown in Figure 2h. Model trials having OL, AA, and NA in the basis set do not significantly reduce the size of the residual, which is consistent with low levels of these compounds after reaction. The three major peaks in the residual at 1740, 1095, and 940 cm^{-1} may correspond to polymeric ester products. The residual, however, should not be considered the true infrared spectrum of the products because of strong nonorthogonal relationships in the infrared spectra, as seen directly in the infrared spectra of the pure compounds and as implied by the absence of C−H absorbance from 2700 to 3000 cm^{-1} in the residual. The nonorthogonal relationships develop because of the common functional groups and structures (i.e., *n*-alkane backbone with terminating aldehyde and carboxylic groups) of the reference and product compounds.

3.4.2. Ozonolysis Kinetics. The time evolution of absorbance is shown in Figures 12 and 13 (300 and 30 ppm O_3, respectively) for the four spectral regions characteristic of C−O bonds, C−C bonds, C═O bonds of ketones, aldehydes, and carboxylic acids, and C═O bonds of esters. Exponential fits are shown. The rate coefficient for C═O loss of 0.147 min^{-1} (Figure 12c, infrared

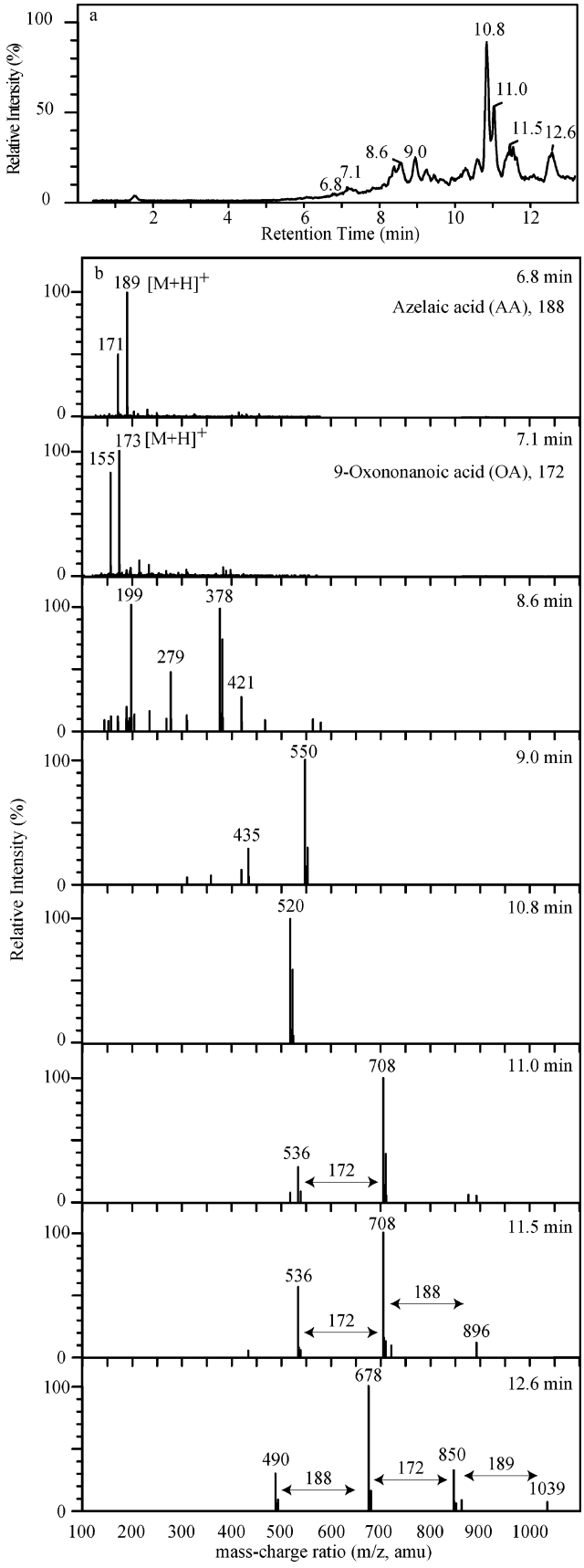

Figure 10. (a) HPLC−MS chromatogram of acetonitrile-soluble constituents of oleic acid droplets after reaction with ozone (90 min). (b) Electrospray mass spectra for the peaks shown in the chromatogram. Azelaic acid and 9-oxononanoic acid are identified. Six peaks with high mass are unidentified. Control runs show that this method is not sensitive to 1-nonanal, nonanoic acid, and oleic acid. Conditions: same as Figure 8.

analysis) can be compared to the rate coefficient for the loss of oleic acid of 0.12 min^{-1} (Figure 9, chromatography analysis). The rate coefficients, which are shown in Figures 12 and 13, are approximately 10 times lower for 30 ppm O_3 than those for 300 ppm O_3. Quadratic forms also fit the infrared data well; mechanistic implications of exponential versus quadratic fits to the data are discussed by Hearn et al.[14]

Data points not included in the exponential fits (shown by markers ×) in Figure 12 and especially in Figure 13 clearly show a two-step time behavior, for which the exponential fit applies to the second step. In particular, Figures 12c and 13c show that the C═O absorption by aldehydes, ketones, and carboxylic acids at first increases and then decreases. Moreover, the time period of the first step is not linear in O_3 concentration (e.g., 2 min in Figure 12c for 300 ppm O_3 compared to 90 min in Figure 13c for 30 ppm O_3). The two-step kinetic behavior suggests a complex chemical mechanism involving the buildup of reactive intermediates followed by their loss as the reservoir of reactive double bonds is depleted.

3.4.3. Comparison of Our Results to Previous Reports. In the current study, 1-nonanal, 9-oxononanic acid, nonanoic acid, octanoic acid, azelaic acid, and products having molecular weights of over 1000 amu are identified in the oxidation of oleic acid by ozone. Except for octanoic acid (1% yield), these products have previously been reported in the literature, though at different yields (Table 1). Katrib et al.,[15] Hearn and Smith,[13] Zahardis et al.,[16] Hearn et al.,[14] and Ziemann[17] have previously reported products having molecular weights of over 200 amu. (Maximum instrument capabilities of those studies varied from 300 to 400 amu.) The infrared peak at 1740 cm^{-1}, which was also observed by Asad et al.,[18] is attributed by us to a C═O ester functional group, specifically α-acyloxyalkyl hydroperoxides, which is a product category also reported by Zahardis et al.,[16] Hearn et al.,[14] and Ziemann.[17] One product reported in the literature, 9-oxooctadecanoic acid (1% yield),[13] is not observed by us, although this product may occur but in an amount below our detection limit. Zahardis et al.[16] and Ziemann[17] also found evidence for the formation of diperoxides, although quantitative yields of these products were not obtained.

Reports of the carbon yields for products and the phase partitioning of at least one product (1-nonanal) vary considerably in the literature and also in comparison with the results of the current study. 1-Nonanal is a semivolatile compound, and it has been reported both as a gas-phase product at 25% yield[9,12] and as a combined gas-phase and condensed-phase product at 42% yield.[13] Katrib et al.[15] reported that 1-nonanal has a 0% yield in the condensed-phase. In the current study, 1-nonanal is the most abundant product in the condensed-phase. (Gas-phase products are not analyzed in the current study. Condensed-phase products were not analyzed by Moise and Rudich[9] or Thornberry and Abbatt.[12] Quantitative yields were not reported by Zahardis et al.[16] or Ziemann.[17] Hearn and Smith[13] reported the combined gas-phase and condensed-phase yield of nonanal.)

In addition to 1-nonanal, the yields of other products, as reported both in the literature and in comparison to the results of the current study, also vary (Table 1). The results of our current study give yields of 14% for 9-oxononanoic acid, 6% for azelaic acid, and 7% for nonanoic acid. Katrib et al.[15] reported yields of 20−35% for 9-oxononanoic acid depending on the initial layer thickness (2−30 nm) of oleic acid on coated particles, yields of 1−3% for nonanoic acid and azelaic acid, and a total carbon yield of 75% in the condensed phase. Azelaic acid was observed but not quantified by Moise and Rudich.[9] Nonanal, nonanoic acid, 9-oxononanoic acid, and azelaic acid

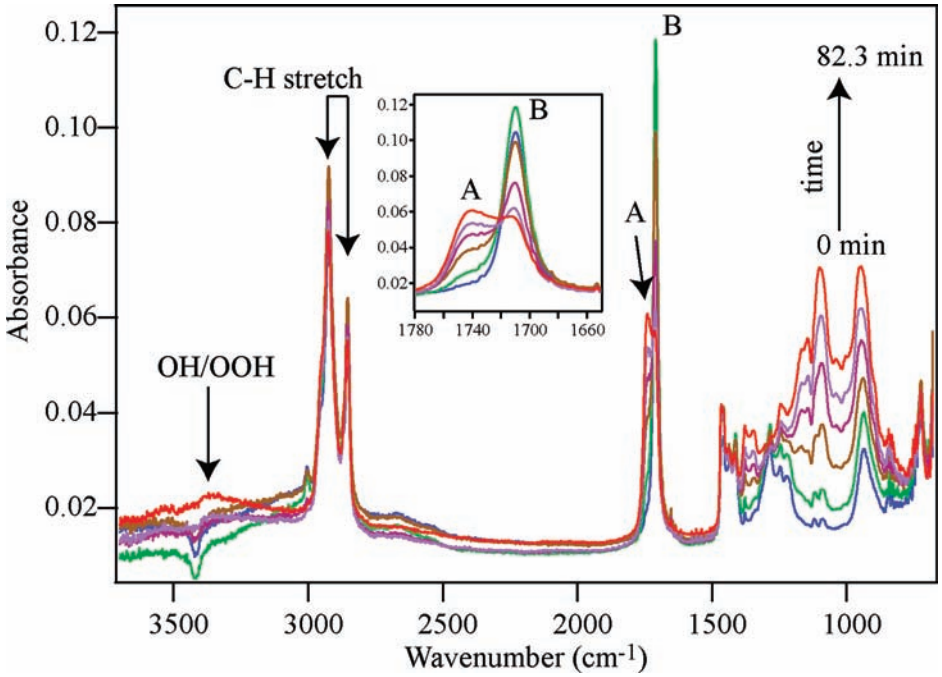

Figure 11. Infrared spectra recorded during the reaction of oleic acid droplets with ozone. The average diameter and volume of the oleic acid droplets are 2.2 mm and 1.5 μL, respectively. Inset: ester C═O vibration, peak *A*; other C═O vibration, peak *B*. Conditions: same as in Figure 8.

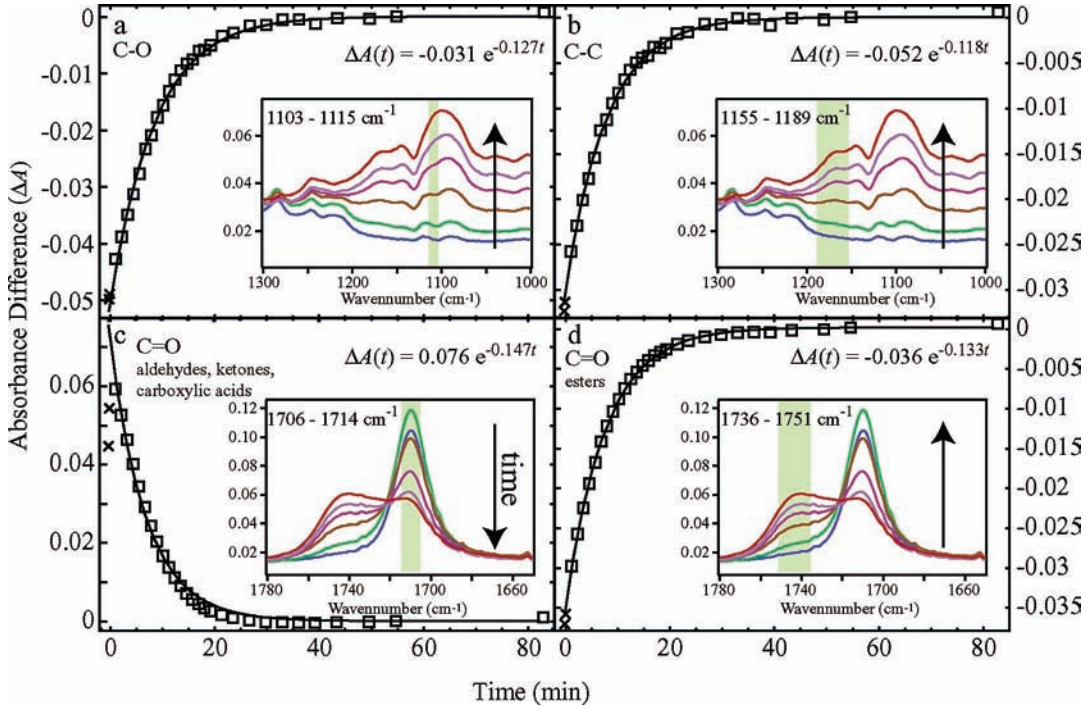

Figure 12. Temporal response of the change in the infrared spectra shown in Figure 11 (300 ppm O_3). Results, shown as the absorbance difference for several spectral windows, are fit to exponential functions $\Delta A(t) = Be^{-kt}$ (solid black line), where *B* is the absorbance difference at time zero and *k* is the first-order rate coefficient. The reference spectrum for the difference calculation is the spectrum recorded at the end of the experiment. Data points shown by the symbol × are excluded from the exponential fit. Insets: expanded spectral region of Figure 11. Highlighting shows the spectral region used to calculate an average absorbance. Conditions: same as in Figure 8.

were observed by Zahardis et al. but not quantified.[16] Hearn and Smith[13] reported yields of 42% for 9-oxononanoic acid, 6% for azelaic acid, and 9% for nonanoic acid.

The following three sections offer possible explanations for the variations among results reported in the literature, especially in regard to products formed and their yields.

3.4.3.a. Influence of the Analytical Method. The detection method influences the reported species, first by bifurcation between the study of gas-phase versus condensed-phase products, second by selectivity toward specific products in the case of condensed-phase analysis, and third by quantitative versus nonquantitative analysis. Some of the discrepancies in Table 1 are explained by the influence of the analytical method. For example, azelaic acid is a nonvolatile product that can be detected and assayed in the AMS as done by Katrib et al.,[15] in a CIMS-based aerosol flow tube as done by Hearn and Smith,[13]

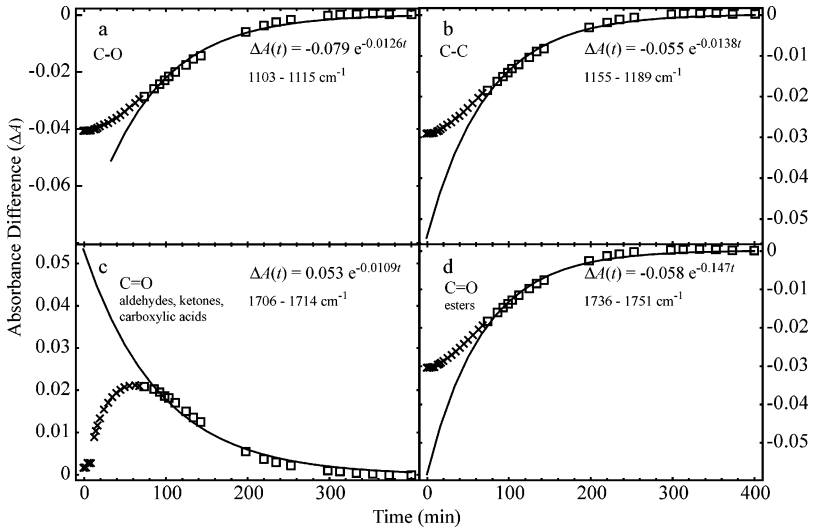

Figure 13. Same as Figure 12 but for decreased ozone concentration (30 ppm O_3). Exponential functions are fit to the data beginning at 90 min. Data points shown by the symbol × are excluded from the exponential fit. Conditions: 1100 mL/min flow of 2% O_2 and 98% N_2. Droplet diameter is the same as in the experiments shown in Figure 12.

in an IC instrument as done by Moise and Rudich,[9] in PERCI-MS by Zahardis et al.,[16] and in an LC−MS instrument as done in this study. In contrast, azelaic acid is not detected by the GC−MS methods of this study.

3.4.3.b. Influence of the Oleic Acid Physical Dimension. Observations of product differences suggest that the physical dimension of oleic acid influences the products formed. The physical dimensions of oleic acid in the experiments reported in the literature (Table 1) are submicron homogeneous aerosol particles,[8,10,13,14,16,17] wall coatings,[9,12] solution reactions in glassware,[17] and nanometer-thick coatings on core particles.[15,20] Bulk reactions dominate for homogeneous aerosol particles and wall coatings whereas surface reactions may be important for nanometer-thick coatings on core particles. A second effect of physical dimensions is the diffusion-based coupling of reagent concentration fields as well as diffusion-based coupling of evaporation and product fields. As an example of the first, oleic acid diffuses rapidly in 100-nm particles and all oleic acid in the substrate may, therefore, be assumed available to react with ozone. The same assumption does not hold for thick coatings on wall. As an example of the second type of coupling, a volatile product such as 1-nonanal in a system of physical dimensions of a 2- to 30-nm coating on a core particle[15] will rapidly diffuse to the surface and evaporate, thus essentially obviating any further condensed-phase reactions such as secondary ozonide formation. In contrast, 1-nonanal in a 800-nm particle[13] may be present long enough for additional reactions.

3.4.3.c. Influence of the Ratio of Moles of Ozone to Moles of Oleic Acid. The ratio of the moles of ozone to the moles of oleic acid can affect product yields. For instance, if this ratio is much less than unity, then the only expected products are those resulting directly from oleic acid ozonolysis (viz. 1-nonanal and 9-oxononanoic acid) and the reaction of the Criegee intermediates with oleic acid. If, on the other hand, the ratio is much greater than unity, then numerous additional reactions of the Criegee intermediates with intermediate products (see section 3.4.4) are expected, including polymerization reactions. Moreover, some of these products may also react with ozone, such as the attack by ozone on carboxylic acid groups, although at much slower reaction rates than ozonolysis of alkenes.

Table 1 shows that the ratios employed in the experiments vary from 10^{-6} to 10^{-10} for some of the coated wall flow tube experiments to much greater than unity for many of the aerosol experiments. For aerosol experiments, the ratio is the concentration of ozone (molecules cm^{-3}) to that of oleic acid (molecules cm^{-3}). For coated wall experiments, the ratio is the molecules of ozone (as given by the product of ozone concentration, flow, and reaction time) to molecules of oleic acid (as given by the mass in the film). A shortcoming is that both of these formulations assume that the ozone and oleic acid are thoroughly mixed, whereas mass transfer may be important, especially in the case of the coated wall experiments.

3.4.4. Proposed Mechanism. An updated mechanism accounting for the new experimental observations is proposed for the ozonolysis of oleic acid droplets (Figures14 and 15). Ozone addition to oleic acid forms a primary ozonide, which decomposes into two stable products and two reactive Criegee intermediates (Figure 14). The products are 1-nonanal and 9-oxononanoic acid, each at 25% carbon yield. The high-energy Criegee intermediates can react by several pathways. They can isomerize to form some of the observed products, including nonanoic acid, azelaic acid, and octanoic acid, although the data show that these are minor pathways. These products, once formed, are as stable as 1-nonanal and 9-oxononanoic acid; therefore, a tenable mechanism should scavenge their precursors, which are the Criegee intermediates.

One pathway for scavenging is that the Criegee intermediates, in the form of carbonyl oxides, react with the carboxylic acids, including oleic acid, 9-oxononanoic acid, nonanoic acid, and azelaic acid, to form α-acyloxyalkyl hydroperoxides,[14,17,21] which contain an ester group (Figure 15). The infrared observations show that the formation of ester groups is a major reaction channel. By this pathway, these esters are expected to be mostly $C_9(O)OC_{18}$ compounds early in the time course of the reaction when Criegee intermediates add to oleic acid, a mix of $C_9(O)OC_9$ and $C_9(O)OC_{18}$ compounds in the middle of the reaction as $C_9(O)OC_{18}$ compounds build up and then undergo ozonolysis to form $C_9(O)OC_9$ compounds, and predominantly $C_9(O)OC_9$ compounds as well as oligomeric $C_9(O)O[C_9(O)O]_nC_9$ compounds at the end of the reaction. The progression through these compounds may explain the two-step kinetic behavior apparent in the infrared observations (Figures 12 and 13).

A second parallel pathway for scavenging, as proposed by Katrib et al.,[15] is that the Criegee intermediates react with the unsaturated double bonds of a different oleic acid molecule to

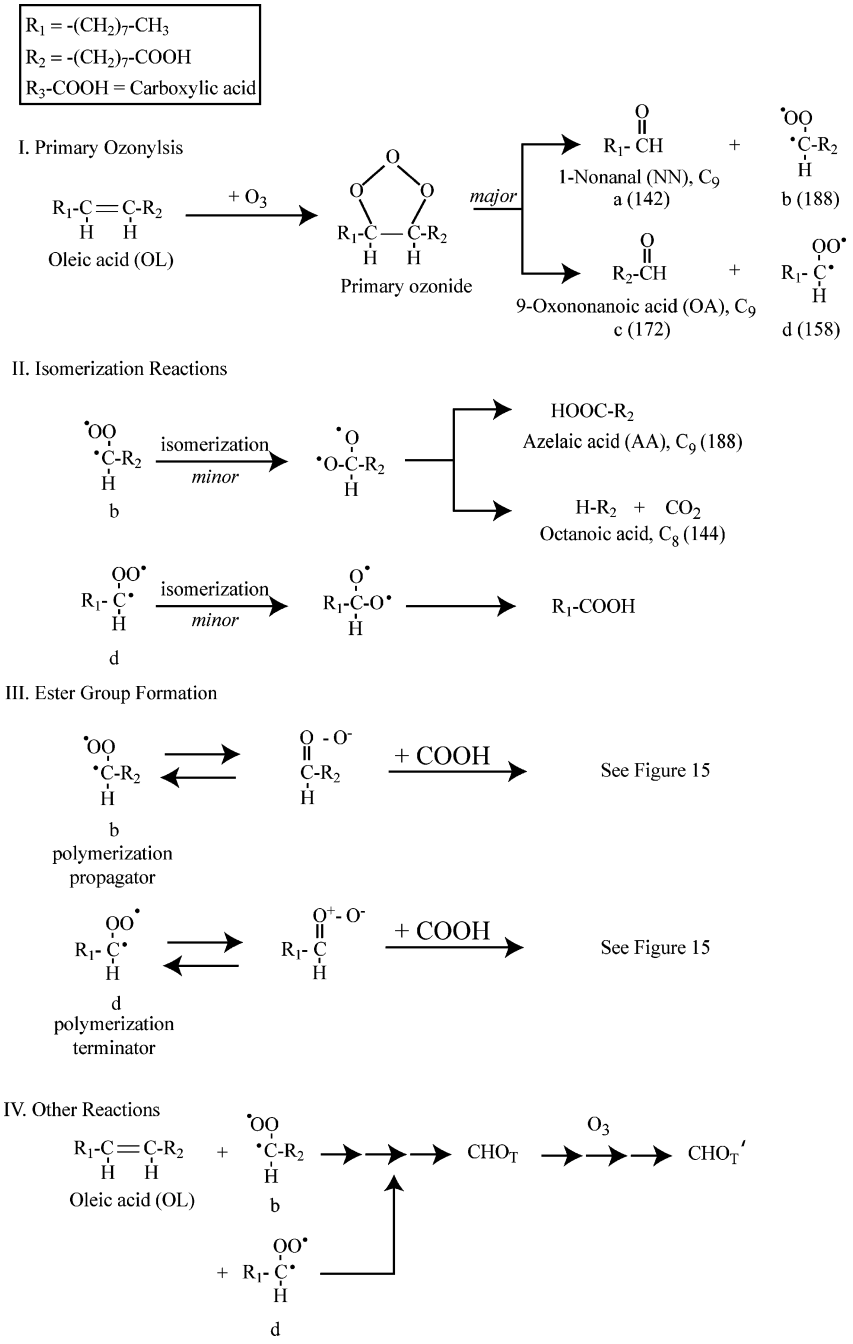

Figure 14. Proposed chemical mechanism for the reactions of oleic acid with ozone.

form C_{27} compounds. The C_{27} compounds subsequently decompose into C_{18} compounds such as 9-oxooctadecanoic acid. This last compound has been observed by Hearn and Smith.[13] Consecutive reaction pathways, such as the formation of a $C_9(O)OC_{18}$ ester followed by Criegee addition across the C_{18} moiety to yield $C_9(O)OC_{27}$ compounds, can lead to compounds of high molecular weight. Subsequent reactions, such as by the hydroperoxide groups of $C_9(O)OC_{9,18,27}$ (i.e., $C_{9,18,27}$ denotes one moiety in the set of C_9, C_{18}, and C_{27}) or secondary ozonide formation by Criegee radical attack on aldehyde groups of $C_9(O)OC_{9,18,27}$ to form $[C_9(O_2)(O)C_9](O)OC_{9,18,27}$, may also play a role in linking additional moieties. The formation of high molecular weight compounds up to 1039 amu is apparent in the mass spectra (Figure 10).

In the proposed polymerization mechanism (Figure 15), 9-oxononanoic acid and the azeleic acid Criegee intermediate are polymerization propagators, whereas 1-nonanal is a released product never incorporated into $C_9(O)OC_{9,18,27}$ and the nonanoic acid Criegee intermediate is a polymerization terminator. For instance, for 9-oxononanoic acid as C_9 in $C_9(O)OC_{18}$, the carbon chain can grow as a secondary ozonide, $[C_9(O_2)(O)C_9](O)OC_9$-$(O)OC_{18}$. To further this example, if the added C_9 is the nonanoic acid Criegee intermediate, then the terminating group is $-CH_3$ and no further reaction by this part of the molecule is expected. In contrast, if the added C_9 is the azelaic acid Criegee intermediate, then the terminating group is $-$COOH, and further esterification is possible to grow the chain, $C_9O(O)[C_9(O_2)(O)C_9]$-$(O)OC_9(O)OC_{18}$. The steps of 172 amu (9-oxononanoic acid) and 188 amu (azaleic acid Criegee intermediate), apparent in the mass spectra in Figure 10, provide evidence of the proposed role of these species as polymerization propagators. The esterfication and secondary ozonide reactions provide pathways for linear polymerization propagation; the addition of a Criegee

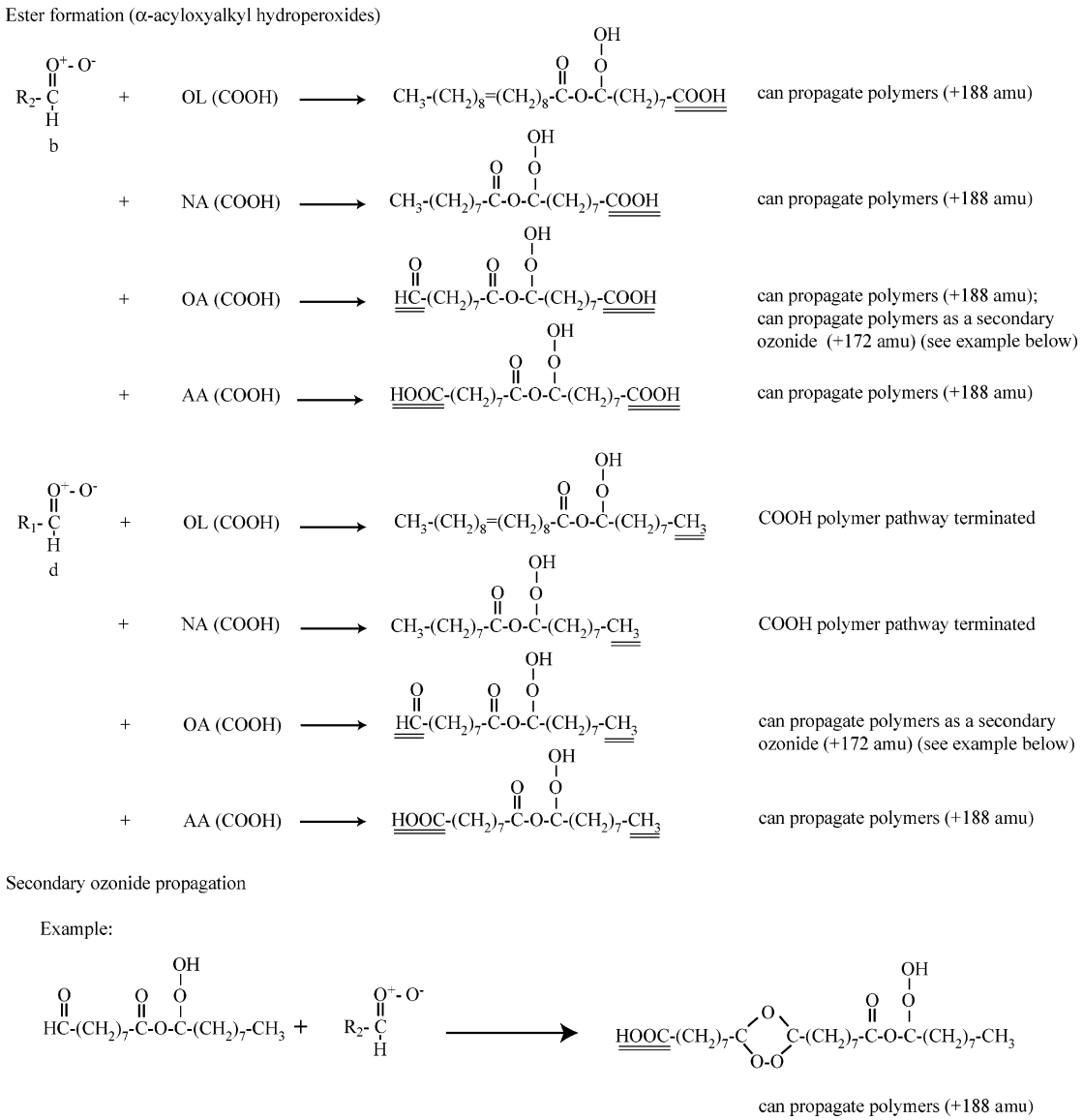

Figure 15. Proposed chemical mechanism for polymerization. 9-Oxononanoic acid and the Criegee intermediate precursor to azelaic acid are the monomers in the condensed-phase polymerization reactions. The effects of the underlined functional groups on propagation or termination of polymerization are noted on the right side of the figure.

intermediate across the double bond of oleic acid provides a pathway for branching propagation.

The findings of Katrib et al.[15] of long chain products are consistent with both the esterification and double-bond-addition pathways. The high observed yield of 9-oxonanoic acid (40% versus 25% by simple pathways in Katrib et al.[15]) is consistent with the double-bond-addition pathway but not the esterification pathway. The relative importance of these two pathways may differ for thin coatings of Katrib et al.[15] and the large droplets employed in the current study. On the basis of observations of product yield with layer thickness, Katrib et al.[15] indeed suggested that the double-bond-addition pathway is favored as a surface reaction. The ozone exposure, which may also affect the relative importance of the pathways, is 1×10^{-5} atm s in Katrib et al.[15] versus 1 atm s in the current study. The ratio of moles of ozone to moles of oleic acid, which are 10^6 and 10^1 in the respective studies, may also influence the relative importance of the reaction pathways.

4. Conclusions

In this study, the oxidation of oleic acid by ozone and nitrate radical was monitored in real time by infrared spectroscopy and off-line via GC−MS and LC−MS analyses for detailed product identification. Moreover, the hygroscopic properties of reacted oleic acid droplets with ozone and nitrate radical were studied using ESEM. Several conclusions reached from this paper's findings contribute to a better understanding of the complexity of the heterogeneous chemistry of unsaturated organics with chemical oxidants:

1. The IR spectra show that the formation of ester groups is a major reaction channel in the ozonolysis of oleic acid. The attack of the Criegee intermediate appears to follow parallel pathways of addition to a carboxylic acid functional group to form an ester (namely, α-acyloxyalkyl hydroperoxide) or addition across a double bond. In addition, Zahardis et al.[16] recently proposed a third pathway for the coupling of two Criegee intermediates to form cyclic diperoxides.

2. Polymerization chain reactions are implicated by 172 and 188 amu motifs apparent in the mass spectra of the high molecular weight products of oleic acid ozonolysis. The polymerization propagators are 9-oxononanoic acid and azelaic acid Criegee intermediate. The formation of high molecular weight products further explains the observed increase in viscosity subject to oleic acid ozonolysis.

3. Reported product yields from oleic acid ozonolysis depend on the analytical methods employed, the physical dimensions of the oleic acid substrate, and the ratio of the moles of ozone to moles of oleic acid. Comparisons of literature results are best understood when these influencing factors are considered.

4. The IR spectra show the formation of $-ONO_2$, $-O_2NO_2$, and $-NO_2$ functional groups when oleic acid droplets are exposed to nitrate radical. High molecular weight products are also observed in the LC−MS measurements.

5. The hygroscopic properties of the unsaturated fatty acid droplets are changed due to the oxidation reaction products. The water uptake RH of the oleic acid droplets is reduced to 91% after exposure to ozone and to 97% after exposure to NO_3. This result of increased hygroscopicity corroborates the reports by Asad et al.[18] and Broekhuizen et al.[19] The increased hygroscopic response of oxidized oleic acid particles suggests that aged organic aerosol particles in the atmosphere may have a considerable impact on particle diameter and, hence, light scattering and radiative forcing. Moreover, changes in hygroscopicity also affect CCN activity and, hence, alter cloud properties (i.e., the aerosol indirect effect).

6. The ratio of moles of oxidant to moles of organic material in atmospheric aerosol particles can be estimated. Ozone concentrations range from 10 to 100 ppb [$(0.25-2.5) \times 10^{12}$ molecules cm^{-3}] under typical boundary layer (i.e., lower troposphere) conditions, and the loading of particulate matter in the accumulation mode ranges from 10 to 100 $\mu g\ m^{-3}$. Under an assumption that this particulate matter is all oleic acid, the corresponding particle loading is $(0.2-2) \times 10^{11}$ molecules cm^{-3}. Moreover, ozone has in situ sources so that its concentration can be renewed, and only a small fraction of the particulate matter is composed of organic alkenes. Therefore, the ratio of the moles of ozone to the moles of reactive particle-phase alkenes is much above unity for typical boundary layer conditions. The implication is that a range of additional reactions, including polymerization, may be favorable inside atmospheric aerosol particles.

7. Although the time course of reactants and products is most accurately described by the numerical solutions to a set of coupled system of differential equations, this approach is cumbersome and often not possible when products and rate constants are not known. In ozonation chemistry, a commonly employed substitute ordinate for progress of reaction is the dosage, given as "atm s". So long as oleic acid is abundant (i.e., the ratio moles of ozone to moles of oleic acid is much less than unity), then parent compound loss and product formation are expected to be linear in the ordinate of "atm s". Therefore, this ordinate has utility in the coated wall experiments or in an organic chemist's beaker. In contrast, when additional reactions become important for a ratio approaching or exceeding unity (such as in the aerosol experiments), the abscissa "atm s" is no longer informative. For interpretation of some aerosol experiments, an ordinate of improved utility may be the ratio moles of ozone to moles of oleic acid. Both of these ordinates are also only of value so long as ozone concentrations are low enough that all significant rates are first order in ozone concentration.

Acknowledgment. We are grateful for support received from the NSF Atmospheric Chemistry Program (ATM 0215357) and the New York Community Trust Merck Fund. Valuable discussion with Richard Schalek is appreciated.

References and Notes

(1) Seinfeld, J. H.; Pandis, S. N. *Atmospheric Chemistry and Physics*; Wiley: New York, 1998.

(2) Rudich, Y. *Chem. Rev.* **2003**, *103*, 5097.

(3) Seinfeld, J. H.; Pankow, J. F. *Annu. Rev. Phys. Chem.* **2003**, *54*, 121.

(4) Saxena, P.; Hildemann, L. M.; McMurry, P. H.; Seinfeld, J. H. *J. Geophys. Res.* **1995**, *100*, 18755.

(5) Facchini, M. C.; Mircea, M.; Fuzzi, S.; Charlson, R. J. *Nature* **1999**, *401*, 257.

(6) Weingartner, E.; Burtscher, H.; Baltensperger, U. *Atmos. Environ.* **1997**, *31*, 2311.

(7) Novakov, T.; Penner, J. E. *Nature* **1993**, *365*, 823.

(8) Morris, J. W.; Davidovits, P.; Jayne, J. T.; Jiménez, J. L.; Shi, Q.; Kolb, C. E.; Worsnop, D. R.; Barney, W. S.; Cass, G. *Geophys. Res. Lett.* **2002**, *29*, 1357.

(9) Moise, T.; Rudich, Y. *J. Phys. Chem. A* **2002**, *106*, 6469.

(10) Smith, G. D.; Woods, I. E.; DeForest, C. L.; Baer, T.; Miller, R. E. *J. Phys. Chem. A* **2002**, *106*, 8085.

(11) Smith, G. D.; Woods, E.; Baer, T.; Miller, R. E. *J. Phys. Chem. A* **2003**, *107*, 9582.

(12) Thornberry, T.; Abbatt, J. P. D. *Phys. Chem. Chem. Phys.* **2004**, *6*, 84.

(13) Hearn, J. D.; Smith, G. D. *J. Phys. Chem. A* **2004**, *108*, 10019.

(14) Hearn, J. D.; Lovett, A. J.; Smith, G. D. *Phys. Chem. Chem. Phys.* **2005**, *7*, 501.

(15) Katrib, Y.; Martin, S. T.; Hung, H. M.; Rudich, Y.; Zhang, H.; Slowik, J. G.; Davidovits, P.; Jayne, J. T.; Worsnop, D. R. *J. Phys. Chem. A* **2004**, *108*, 6686.

(16) Zahardis, J.; LaFranchi, B. W.; Petrucci, G. A. *J. Geophys. Res.* **2005**, in press.

(17) Ziemann, P. J. In press.

(18) Asad, A.; Mmereki, B. T.; Donaldson, D. J. *Atmos. Chem. Phys.* **2004**, *4*, 2083.

(19) Broekhuizen, K. E.; Thornberry, T.; Kumar, P. P.; Abbatt, J. P. D. In press.

(20) Katrib, Y.; Martin, S. T.; Rudich, Y.; Davidovits, P.; Jayne, J. T.; Worsnop, D. R. *Atmos. Chem. Phys.* **2005**, *5*, 275.

(21) Bailey, P. S. Ozonation in Organic Chemistry. In *Organic Chemistry*; Trahanovsky, W., Ed.; Academic Press: London, 1978; Vol. I Olefinic Compounds.

(22) Dekermenjian, M.; Allen, D. T.; Atkinson, R.; Arey, J. *Aerosol Sci. Technol.* **1999**, *30*, 349.

(23) Palen, E. J.; Allen, D. T.; Pandis, S. N.; Paulson, S. E.; Seinfeld, J. H.; Flagan, R. C. *Atmos. Environ.* **1992**, *26*, 1239.

(24) Palen, E. J.; Allen, D. T.; Pandis, S. N.; Paulson, S.; Seinfeld, J. H.; Flagan, R. C. *Atmos. Environ.* **1993**, *27*, 1471.

(25) Davidson, J. A.; Viggiano, A. A.; Howard, C. J.; Dotan, I.; Fehsenfeld, F. C.; Albritton, D. L.; Ferguson, E. E. *J. Chem. Phys.* **1978**, *68*, 2085.

(26) Dlugokencky, E. J.; Howard, C. J. *J. Phys. Chem.* **1988**, *92*, 1188.

(27) Noda, J.; Hallquist, M.; Langer, S.; Ljungstrom, E. *Phys. Chem. Chem. Phys.* **2000**, *2*, 2555.

(28) Finlayson-Pitts, J. B.; Pitts, N. J. J. *Chemistry of the Upper and Lower Atmosphere*; Academic Press: San Diego, 2000.

(29) Thornton, J. A.; Braban, C. F.; Abbatt, J. P. D. *Phys. Chem. Chem. Phys.* **2003**, *5*, 4593.

(30) Cantrell, C. A.; Shetter, R. E.; Calvert, J. G.; Tyndall, G. S.; Orlando, J. J. *J. Phys. Chem.* **1993**, *97*, 9141.

(31) Wangberg, I.; Etzkorn, T.; Barnes, I.; Platt, U.; Becker, K. H. *J. Phys. Chem. A.* **1997**, *101*, 9694.

(32) Ebert, M.; Inerle-Hof, M.; Weinbruch, S. *Atmos. Environ.* **2002**, *36*, 5909.

(33) Noda, J.; Ljungstrom, E. *Atmos. Environ.* **2002**, *36*, 521.

(34) Noda, J.; Nyman, G.; Langer, S. *J. Phys. Chem. A* **2002**, *106*, 945.

(35) Noda, J.; Holm, C.; Nyman, G.; Langer, S.; Ljungstrom, E. *Int. J. Chem. Kinet.* **2003**, *35*, 120.

(36) Wayne, R. P. *Atmos. Environ.* **1991**, *25*, R5.

(37) Hallquist, M.; Wangberg, I.; Ljungstrom, E.; Barnes, I.; Becker, K. H. *Environ. Sci. Technol.* **1999**, *33*, 553.

(38) Allen, D. T.; Palen, E. J.; Haimov, M. I.; Hering, S. V.; Young, J. R. *Aerosol Sci. Technol.* **1994**, *21*, 325.

(39) Urban, M. W. *Attenuated Total Reflectance Spectroscopy of Polymers: Theory and Practice*; American Chemical Society: Washington, DC, 1996.

(40) Pramanik, B. N.; Ganguly, A. K.; Gross, M. L. *Applied Electrospray Mass Spectrometry*; Marcel Dekker: New York, 2002.

(41) Atkinson, R. *Int. J. Chem. Kinet.* **1997**, *29*, 99.

(42) Kriz, P. L. *Introduction to Organic Laboratory Techniques*; Saunders College Publishing: Philadelphia, 1999.

(43) Moise, T.; Rudich, Y. *J. Geophys. Res.* **2000**, *105*, 14667.